Logarithmic Type Image Processing Framework for Enhancing Photographs Acquired in Extreme Lighting

Corneliu FLOREA, Laura FLOREA
Image Processing and Analysis Laboratory(LAPI),University Politehnica Bucuresti, Romania
corneliu.florea@upb.ro

Abstract—**The Logarithmic Type Image Processing (LTIP) tools are mathematical models that were constructed for the representation and processing of gray tones images. By careful redefinition of the fundamental operations, namely addition and scalar multiplication, a set of mathematical properties are achieved. Here we propose the extension of LTIP models by a novel parameterization rule that ensures preservation of the required cone space structure. To prove the usability of the proposed extension we present an application for low-light image enhancement in images acquired with digital still camera. The closing property of the named model facilitates similarity with human visual system and digital camera processing pipeline, thus leading to superior behavior when compared with state of the art methods.**

Index Terms—**Digital cameras, Image processing Image enhancement, Linear algebra.**

I. INTRODUCTION

In the recent years, digital still cameras (DSC) have sufficiently evolved so to become compact and cheap enough to be used way beyond simple photography. In the consumer range, the miniaturization trend reached a pinnacle with Mobile Phone Cameras. In the same time their distribution was broadly enlarged in various fields of industry like automotive or game industry, etc. While, the camera producers engage with tremendous efforts in the megapixels race, the trend of miniaturization is imposing design modifications such as reducing the size of optics and of photo-sensible area, which lead to more pressure on the image processing pipeline, especially if new features are added. In this paper we introduce a parametric extension of existing models for image processing that provides a suitable framework for enhancing the functionality of typical digital cameras in extreme lighting conditions. To be more precise, we will describe methods for enhancing images acquired in low lighting (which is a solution to motion-blur degradation of images due to shaky hands).

The Logarithmic Type Image Processing models represent an alternative to image processing with real based operations. Under certain circumstances, such a combination, named Classical Linear Image Processing (CLIP) - [1] proves its limitations like the upper range overflow which is often brutally solved by truncation. Consequently, more elaborate structures appeared, namely Logarithmic Image Processing (LIP) models [2], [3]. More

recently the logarithmic model has been replaced by a logarithmic-like one with the benefits of a simplified calculus [4] (to form the class of logarithmic type image processing – LTIP) and these models were enriched with parametric extensions [5], [6]. While these models required additional constraints, the set of simple rules that guarantee the algebraic model of a cone space introduced in [7], [8] permits a more robust parameterization. The structure of a vector or a cone space includes the property of closing which enforces a similarity with the human visual system, trait that also exists in the digital camera. We will exploit this similarity while constructing a method for low light image enhancement.

The remainder of the paper is organized as follows: in the next section the mathematical background of the LTIP models is reviewed, as well as the new parametric extension. Section III reviews the global description of the image processing pipeline for DSC platforms. Section IV describes how we can use the closed logarithmic-like amplification and addition to provide an efficient solution for low-light image acquisition. The application is a core one for a DSC platform and we will discuss the achieved results in section V. Finally, section VI summarizes the proposed solutions and discusses further continuations paths.

II. LOGARITHMIC TYPE IMAGE PROCESSING MODELS

The mathematical construction of a LTIP model may start by defining the operational laws (the addition and the scalar multiplication) or, equivalently, by finding the function that maps the investigated model definition set onto the real number algebraic structure, hence acting as a generative mapping. We follow the procedure from [7], [8] namely focusing on the second alternative and in the next subsections we will review results that define a set of conditions that guarantees achieving a vector (cone) space structure. We must stress that this is an algebraic exercise applied on image processing domain.

A. Vector/Cone Space Structure

Let us consider a function, $\Phi : D_\Phi \to E$. Within this choice, the set D_Φ is the uni-dimensional image definition set. For color (multi-dimensional) images, the discussion may refer to each plane independently. Typically, if the image values have intensity meaning, the set is bounded (e.g. the values are in the [0,255] range).

The function Φ defines the model structure and maps the

image definition set, D_Φ, onto a subset of real numbers, *E*. Following the theory elaborated by Oppenheim, [9], [10], the two basic operations (addition of two elements of the set, $\oplus$, and multiplication, $\otimes$, with an outer, typically real scalar α) are defined over the given set, D_Φ, as following:

$$\Phi(u \oplus v) = \Phi(u) + \Phi(v) \quad (1)$$

$$\Phi(\alpha \otimes u) = \alpha \Phi(u) \quad (2)$$

where $u, v \in D_\Phi$ and $\alpha \in K \subset \Re$.

Equations (1) and (2) are the defining conditions of a homomorphism between two similar algebraic structures. The simplest solution is to consider the function Φ a bijection and, hence, to have the laws uniquely determined.

With respect to the bijectivity constraint (thus, the existence of Φ^{-1}), the definition laws are determined by:

$$u \oplus v = \Phi^{-1}(\Phi(u) + \Phi(v)) \quad (3)$$

$$\alpha \otimes u = \Phi^{-1}(\alpha \Phi(u)) \quad (4)$$

A set of sufficient conditions that need to be fulfilled by a generative function so to produce a usable logarithmic-type image processing model is:

- Φ should be bijective;
- The target E should be at least $[0; +\infty)$ in the case of cone structure;
- $\Phi(u_0) = 0$.

Of practical importance for the LTIP models is the closing property of both addition and scalar multiplication. This states that the sum of any two images should lead to another valid image and, respectively, any amplified or attenuated image should be an image:

$$\forall u, v \in D_\Phi, z = u \oplus v \Rightarrow z \in D_\Phi$$
$$\forall u \in D_\Phi, \forall \alpha \in K, z = \alpha \otimes v \Rightarrow z \in D_\Phi \quad (5)$$

Given the two operative laws, $\oplus$ and $\otimes$, the vector set D_Φ and the outer scalar set *K*, the formal definition of the vector space implies several properties (see [11], section II.1). More precisely the vector addition has to be associative, commutative, should have neutral element and inverse element, while the scalar multiplication should be distributive with respect to vector addition in the fields of vectors and in the fields of scalars, should respect field multiplication and have identity element. These properties do hold under the bijectivity constraint [7].

The existence of the addition identity element, u_0, implies further conditioning over the mapping function, Φ as a consequence of the isomorphic behavior:

$$\forall u \in D_\Phi, \exists u_0 \in D_\Phi, u \oplus u_0 = u \Leftrightarrow \Phi(u_0) = 0 \quad (6)$$

The existence of addition inverse element, u^- is conditioned by a symmetry towards 0 of the generative function. This property makes the difference between vector and cone space. However, since this is not of paramount importance for practical applications, in many cases, the LTIP model has a cone structure.

Similarly with addition, the identity element of the scalar multiplication has to be 1:

$$\exists \alpha_1 \in K, \forall u \in D_\Phi - \{u_0\}, \alpha_1 \otimes u = u \Leftrightarrow \alpha_1 = 1 \quad (7)$$

For models that have a cone space structure, the subtraction is defined as follows:

$$u \Theta v = \Phi^{-1}(\Phi(u) - \Phi(v)) \quad (8)$$

where *u* is enforced to be larger than *v, u>v*

B. Overview of existing models and their applications

The first logarithmic model has been proposed by Jourlin and Pinoli, [12], [2]. They have started from the cascade of two light-transmitting filters to deduce the equation for logarithmic addition and subsequently derived the scalar multiplication. The model was further used in various applications, like background removing [13], image enhancement (contrast and sharpness improvement) [14], [15] and so on. If initially the model has been dedicated to gray-scale image only, soon applications for color image representation and processing appeared [16]. Extensive studies of up-to-the day advances and applications for the LIP may be found in [15] and more recently in [17]. Later advances witness Deng interpretation of the LIP model from an entropy point of view [18] and proof of similitude with the Giga-vision image sensor [6].

In the same time, several other L(T)IP models have been proposed. Pătraşcu, [3] built his model from a mathematical point of view, aiming at a fully developed vector space, while Vertan described a computational simpler logarithmic-like model. Additional results regarding possible generative functions are presented in [7], [19]. All these models, from a mathematical point of view are covered by the formulation proposed in the previous section. The current basic models (that have been showed to be useful for image processing applications, [2], [3], [4]) are summarized in Table 1.

The extension of the LTIP models to color images is trivial since the computation takes place independently on each plane [14]. The same approach will be assumed in this paper too.

C. Parameterization

The basic result used by us to extend the LTIP models by parameterization comes from the algebraic theory (see [11], section III.2). It states that the composition of two valid homeomorphisms leads to another homomorphism [7]. Let be $\psi: D_\Phi^1 \to D_\Phi^2$, a homomorphism from D_Φ^1 to D_Φ^2 and let $\phi: D_\Phi^2 \to E_2$ be a homomorphism from D_φ^2 to E_2, then the composite function $\rho = \phi \circ \psi = \phi(\psi)$ is a homomorphism from D_φ^1 to E_2. With such a construction, we choose ϕ to be the generative function, Φ, of a known LTIP model and ψ any real function with bounded domain and target set; the result is a valid new LTIP model. One may go even further: it is not really necessary to have the ψ function a homomorphism, but only a bijective function; even in such a case the result is a valid generative LTIP model function.

TABLE 1. SOME OF THE EXISTING LOGARITHMIC TYPE IMAGE PROCESSING MODELS WITH BASIC OPERATIONS. D IS THE UPPER BOUND OF THE IMAGE DEFINITION SET (TYPICALLY D = 255).

Model	Domain	Addition
	Isomorphism	Scalar multiplication
Jourlin [2]	$D_\Phi = (-\infty, D]$ $\Phi_J(x) = D\log\dfrac{D}{D-x}$	$u \oplus v = u + v + \dfrac{uv}{D}$ $\alpha \otimes u = D - D\left(1 - \dfrac{u}{D}\right)^\alpha$
Pătraşcu [3]	$D_\Phi = (-1,1)$ $\Phi_P(x) = \log\dfrac{1+x}{1-x}$	$u \oplus v = \dfrac{u+v}{1+uv}$ $\alpha \otimes u = \dfrac{(1+u)^\alpha - (1-u)^\alpha}{(1+u)^\alpha + (1-u)^\alpha}$
Vertan [4]	$D_\Phi = [0,1)$ $\Phi_V(x) = \dfrac{x}{1-x}$	$u \oplus v = 1 - \dfrac{(1-u)(1-v)}{1-uv}$ $\alpha \otimes u = \dfrac{\alpha u}{1+(\alpha-1)u}$

TABLE 2. PARAMETRIC LTIP MODELS. NOTE THAT PANETTA MODEL HAS A CONE SPACE STRUCTURE ONLY IF $\gamma(D) = \Lambda(D)$ WHILE DENG MODEL ENFORCES $\Phi(x+y, D) = \Phi(x, D_x) + \Phi(y, D_y)$ TO ACHIEVE THE SAME STRUCTURE

Model	Isomorphism	Addition
		Scalar multiplication
Panetta [22]	$\Phi(x) = -\Lambda(D)\cdot$ $\cdot\left(\log\left(1 - \dfrac{x}{\Lambda(D)}\right)\right)^\beta$	$u \oplus v = u + v + \dfrac{uv}{\gamma(D)}$ $\alpha \otimes u = \gamma(D) - \gamma(D)\left(1 - \dfrac{u}{\gamma(D)}\right)^\alpha$
Deng [18]	$\Phi(x, D_x) =$ $-D\log\left(1 - \dfrac{x}{D_x}\right)$	$u \oplus v = D\left(\dfrac{u}{D_u} + \dfrac{v}{D_v} + \dfrac{uv}{D_u D_v}\right)$ $\alpha \otimes u = D\left(1 - \left(1 - \dfrac{u}{D_u}\right)^\alpha\right)$
Current	$\Phi_m(x) = \dfrac{x^m}{1-x^m}$	$u \oplus v = \sqrt[m]{1 - \dfrac{(1-u^m)(1-v^m)}{1-u^m v^m}}$ $\alpha \otimes u = u\exp\left(\dfrac{1}{m}\log\dfrac{\alpha}{1+(\alpha-1)u^m}\right)$

The parameterization is naturally achieved if the ψ function is a parametric function that in all the cases uses the same sets. Such an example may be the family of bijective "power(gamma)-type" functions [7]:

$$\psi_m : [0,1) \to [0,1), \psi_m(x) = x^m, \forall m \in (0, +\infty) \quad (9)$$

Composing this family of functions with the generator mapping of the Vertan logarithmic-like model, [4], a set of parametric LTIP models with the base function is obtained:

$$\Phi_m : [0,1) \to [0, +\infty), \Phi_m(x) = \Phi(\psi_m(x)) = \dfrac{x^m}{1 - x^m} \quad (10)$$

The inverse function is:

$$\Phi_m^{-1}(y) = \psi_m^{-1}(\Phi^{-1}(x)) = \sqrt[m]{\dfrac{y}{1+y}} \quad (11)$$

The mathematical formulas of the so-generated model are found if one replaces formulas (10) and (11) in equations (3), (4) or (8). Hence, the addition $\oplus_m$ becomes:

$$u \oplus_m v = \sqrt[m]{1 - \dfrac{(1-u^m)(1-v^m)}{1-u^m v^m}} \quad (12)$$

The detailed form of the subtraction, Θ_m, is:

$$u\Theta_m v = \sqrt[m]{\dfrac{u^m - v^m}{1 + u^m v^m - 2v^m}} \quad (13)$$

Scalar amplification is:

$$\alpha \otimes u = u\exp\left(\dfrac{1}{m}\log\dfrac{\alpha}{1+(\alpha-1)u^m}\right) \quad (14)$$

We have to note that the "power" function is the hereby choice and any other bijective parametric function will do.

In the used case, for *m=1* the logarithmic-like model is obtained.

D. Relation with other parametric extensions of the LIP models

The first significant result in parameterization of LIP models may be considered the one reported by Panetta et al. [5], [20]. They proposed a parametric extension of the Jourlin model, named PLIP (see table II for details) by replacing the upper bounds with affine transformation with parametric coefficients. The introduction of the parameters offers greater flexibility for defining the new operations but with the cost of losing the cone space structure. In the same time, the Panetta model, if $\gamma(D) \neq \Lambda(D)$ is no longer an extension of Oppenheim's homomorphic systems [9].

Another parameterization has been introduced by Deng [18]. He extends Jourlin model in the framework of homomorphic theory [9], which he calls GLIP (Generalized LIP), using the similarity of Jourlin model with the Giga-vision sensor. The resulting effect is similar with the one produced using the hereby framework. A summary of the parametric LTIP models may be followed in table II.

We note the previous models require additional (and not intuitive) constraints in order to preserve the algebraic structure. Thus the procedure discussed in section II. A is critical when detailing a new extension of the LIP models. Furthermore, we stress that current parametric extension always follows the homomorphic theory and is simpler than Gigavision based model.

III. DIGITAL STILL CAMERAS

The acquisition of images relies on the auto-exposure and autofocus algorithms. While the for the current work only the auto-exposure algorithm, we will refer to the excellent

paper by Ramanath et al. [21] for further details on image processing pipeline in DSC.

The auto-exposure algorithm relies on the APEX equation [22]:

$$E_V = -\log_2 t + 2\log_2 N = \frac{B \cdot S}{K} \quad (16)$$

where E_V is the exposure value, the log_2t forms the time value (T_V), N is the relative diaphragm opening (that is formed by taking the log, the aperture value, A_V), B is the incident light, S is the sensors sensibility (or for digital cameras – the "ISO" amplification) and K is a constant specific to the camera model. Given the scene (i.e. incident light), camera adjusts the other parameters to balance equation (16). In general, two out of the three parameters (exposure time, aperture value and amplification) are kept fix and the third is adjusted so that the reported image intensity in an area of interest forms a Gaussian-like histogram with the mean equal with half of the values range. A description of the typical exposure algorithm may be found in [23], chapter 19.

Regarding the image post-processing, the following main steps are usually required to transform the raw image provided by the sensor into a final one [21], [24]: flawed pixel correction, white balance, de-mosaicing, tone/gamma correction, color correction and color transform.

A. Camera Response Function

The entire camera processing system is typically modeled by the so-called Camera Response Function (CRF). The function takes as input the relative scene objects reflectance and outputs the reported digitized image intensities. The subject of estimating the camera response function has been widely debated in literature. The first attempts were based on taking a single exposure of a uniformly illuminated chart containing patches of known reflectances, such as the Gretag Macbeth chart [25]. The Gretag Macbeth Color Checker provides a subject scene with uniform patches and intensity varying over the entire range of interest. The CRF is estimated in the given set of brightness values and interpolated in the rest. However, the process is quite complicated and can only be performed in restrictive conditions (e.g. the environment illumination must remain un-changed), which are not always accessible.

Later attempts were based on the Debevec and Malik observation, [26], which states that a set of differently exposed images contain, usually, enough information to recover the CRF (denoted here by g) using the images themselves.

If the scenario conditions include the same scene, aperture number and sensors amplification as constants, then the measured intensity is linearly dependent of the exposure time. To be more precise, let us assume that images F_A and F_B of the same scene were photographed with different exposure times T_A and, respectively, T_B. Given a photo-detector, its charge from the two images must have the same ratio as the one between the exposure times. Now, if we come to the reported pixel values u_A and u_B, we get the basic CRF equation:

$$g(u_B) = \frac{T_B}{T_A} g(u_A) \quad (17)$$

Recovering g from the equation (17) is a difficult task, [27] and certain restrictions have to be imposed on g. Mann and Picard, [28], proposed a gamma-like function for g, while Mitsunaga and Nayar, [29], used a low degree polynomial regression.

IV. AMPLIFICATION OF UNDEREXPOSED IMAGES

Nowadays, strong directions of developing DSCs seem to be that of decreasing the size of the camera module and increasing the resolution.

The miniaturization imposes design modifications such as reducing the size of optics and of photo-sensible area, which increases the chance of images to blur from shaking hands [30]. The small photo-sensible area diminishes the number of collisions in the photo-voltaic effect and, therefore, it reduces the correlation between the incident light and the reported image intensity. On the other hand, the small photo-sensible area decreases picture angle. Since human hand jitter is always present, the small picture angle increases the chances that the relative motion between the camera and the scene during exposure time becomes larger than a pixel size and thus leading to visible motion blur. Because this phenomenon can significantly degrade the visual quality of images, photographers and camera manufactures are frequently searching for methods to limit its effects.

An abundance of proposed solutions to the mentioned problem do exist. We may divide these approaches in two categories. The first category tries to eliminate the effects of the motion blur, meaning that there will be a normal image acquisition (with a long enough exposure time that includes blur) and subsequently camera trajectory is estimated in order to restore the blur. The restoration and the estimation processes may be simultaneous and real-time (the so-called optical image stabilization, [31]) or consecutive and digital (by means of deconvolution). However this alternative implies the use of motion sensors and heavy computation (which comes as an extra circuit) and therefore contradicts the size-diminishing goal.

The second approach works on avoiding the circumstances that generate motion blur. This is achieved by reducing the exposure time below the "motion limit". The motion limit may be based on the "*q over f35*" rule of thumb [32] or dynamically deduced from computing the misalignment on consecutive frames for more precise indication of camera motion [33]. This alternate solution may be easily implemented on existing digital camera hardware, without any changes in the acquisition process. However, if such a solution is chosen, the under-exposed image must be amplified so to provide proper luminance and color saturation level. This amplification consists of pixel-based multiplication and it must avoid introducing artifacts that will decrease the perceived image quality [34] and [35].

The hereby proposed solution falls into this category. If the amplification takes place on an image resulting after the processing pipeline, then the amplification should be governed by the camera CRF. Motivated by the similarity

between the CRF and LTIP amplification (discussed in the next subsection), the low-light enhancement algorithm should be implemented in a LTIP framework.

A. Relation of the CRF with LTIP amplification

Beyond avoiding brutal truncation while amplifying, further motivation for the use of the LTIP in such framework lies in the fact that LTIP amplification is a good approximation of the DSC's CRF.

The initial reason that LTIP amplification is an exposure compensation algorithm traces back to the fact that both (camera model and LTIP) were built to follow Weber's law. This law, [36], describes the response of the human eye to a linear variation of the stimulus as being logarithmical. The consistency with Weber's law is one of the properties of the initial model proposed by Jourlin, fact thoroughly demonstrated in [2]. It was also shown that logarithmic subtraction (and hence addition and multiplication) is consistent with Fechner's law of (non-linearity of human) perception [15].

In parallel, the DSC camera incorporate a gamma correction function ([24] – section 8.1.4), which is the main source of the gamma-like shapes of the CRF, noted by Grossberg and Nayar [37]. A set of eloquent examples may be followed in the mentioned paper. The explanation may be in the aimed consistency with older film camera (which were specifically build to follow Weber's law), but there is another, more modern, which is based on adaptation to the human visual system [38]. The basics come from Stevens effect [39], which states that while light becomes more intense, the perception of lightness contrast increases. This means that a visual quanta in the domain of low light is significantly larger than in the high light domain. Since the image acquired by regular image sensor is near linear with respect to image intensity ([24], section 3.4.2.1), to adapt the camera's reported intensity to human visual system there is need for a non-linear distribution of intensities (smaller density in low light domain and larger density - compression at high luminance) followed by uniform quantization. The function that achieves the non-linear compression is a gamma-like function.

The closing property of the LTIP models implies that no matter how strong the input is, the response will always be in the same domain. With respect to reported luminance this means small density of values in domains close to the origin and high density (small quanta) in the upper domain. The similarity between LTIP multiplication, a gamma function and CRF function of camera used in this section may be followed in Fig. 1.

However, observing the results reported by [37] and the ones plotted in Fig. 1, the cameras use the same shape of CRF, but there are differences among various models. To keep the algorithm unitary we used a parametric LTIP model that for various parameters is capable of coping with different CRFs.

Furthermore, we will note that Stevens [39] challenged the Weber-Fechner logarithmic curve of perception and argued for a gamma-shaped. As said, a gamma curve is implemented in DSC. This motivates to extract our parametric model from Vertan logarithmic-like model and not from the older, purely logarithmic ones.

B. Determination of image amplification parameter

First we have to deal with the challenge of selecting the amplification curve that approximates best a specific camera
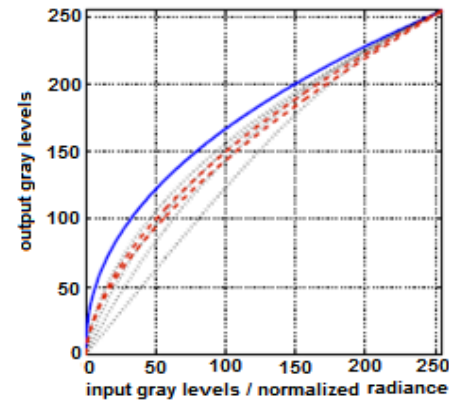

Figure 1. Representation of multiplication (with 0.2 0.5, 1, 1.3 scalars) with the proposed LTIP model (black dotted lines), gamma (γ=0.45) function (solid blue line) and CRF of the a two DSCs used here (red dashed lines). On the X axis we represented we represented input luminance (gray level) and on the Y axis output luminance. The CRFs were approximated with gamma functions as in [28].

CRF. This procedure is similar with the one proposed in [25] and should be done once for a camera model. To be more precise, images with various relative exposure of the Gretag Macbeth chart are taken and a search for the "best" value of the parameter m is performed. The "best" value is chosen as the value that minimizes the mean square error $\overline{\varepsilon_m^2}$:

$$\overline{\varepsilon_m^2} = \sum_{E_V} \sum_P \left(\overline{I_{ref}(P)} - \left(2^{-Ev}\right) \otimes \overline{I_{E_V}(P)} \right)^2 \qquad (18)$$

where P stands for one of the 24 color patches from the Gretag Macbeth chart, $\overline{I_{ref}(P)}$ is the average value of the pixels from the chosen patch of the reference image (i.e. image normally exposed, with parameters that balance eq. (16)), the multiplication $\otimes_m$ is done according to (14), while E_V is the relative exposure of the investigated image. Normally we search in the {±2; ±1; ±0.5; +0.5; +1; +2;} range of relative exposures. Various values for m produce different values for $\overline{\varepsilon_m^2}$. The choice will be the argument that produces the minimum error. The obtained m parameter will be used in all operations that involve LTIP model.

C. Low Light Image Enhancement

It is a known fact that underexposing and amplifying is a solution for reducing the exposure. The camera computes the exposure time using eq. (16). A typical low-light enhancement method firstly captures an image with a short exposure time, ensuring that the image is hand motion free. Next, the image is amplified until its luminance and color levels match the reference extracted from equation (16).

The method works in two steps: global underexposing compensation and local adaptation. The motivation for splitting our method lays in the similarity with human perception. First we quote Dunn et al. [40] that observed that global visual adaptation is completely a retinal process and we follow Stevens model for this part. Next visual

information is processed in the visual cortex for local adaptation/contrasting - see Hubel's book [41], Ch. 4 for a discussion on this topic.

In the underexposing compensation step, we amplify the input image with 2^{-Ev} using equation (14). In the local adaptation step, we correct the previously amplified image so to obtain a specific statistic in small subsets of the image. To formalize the algorithm, let us denote the low-light image with $F(i,j)$. Then, the estimate of the reference image (denoted by $G(i,j)$) is found as:

$$G(i, j) = \left(c_1 \otimes_m F(i, j)\right) \oplus_m c_2(i, j) \qquad (19)$$

The parameter was determined by the method described in section IV. B. The c_1 factor comes from the opposite of the relative underexposure $c_1=2^{-Ev}$ and the amplification stands for underexposure compensation. The amplification is computed with the same c_1 value for the entire image.

The addition with c_2 represents the local adaptation. In this step, the image is divided in smaller rectangular adjacent areas and, independently, for each such patch we find a value for c_2. The search process is an iterative approximation where the aimed value is the one that needs transform best the histogram of the patch of $F_1 = \left(c_1 \otimes_m F\right)$ image into a target histogram. The purpose of this step is to increase the visibility of small objects. At the end, in order to prevent creating fake edges, the c_2 image is highly blurred.

V. IMPLEMENTATION AND RESULTS

Experimental tests showed that a good compromise is obtained if the rectangular pieces used for determination of c_2 have the tenth part of the image size and the blur kernel is twice this value. Theoretically the search for c_2 should be as elaborate as possible; however, practical results showed that restricting the possible values domain to {-40;-25;-12;0;+12; +25;+40} works well enough; the restriction of the range allows to speed up computation with the use of Look-Up-Tables (LUT) for the possible values of the function $f(u) = u \oplus_m c_2$, where u is a intensity level. Furthermore, since the operation is pixel–wise, trial and error procedure should be applied on the histogram of the F_1 image. The tests showed that the objective function (which is the mean square error between the obtained histogram and the aimed histogram – Gaussian with 128 mean and 40 variance) is uni–modal, hence to reduce the number of steps a simple Hill Climbing [42] procedure is implied.

For demonstration purposes, we considered a low-light landscape type scene (Fig. 2) and a still one (Fig. 3). The reference image (showed in subplot (a)) and original image (in subplot (b)) were obtained with a consumer camera. The under-exposed subject image (b) was obtained by forcing the exposure value to be E_V=-1. The ideal image (a), which is not affected by motion blur, was recorded with a tripod mounted camera. The results are showed in subplot (c) where subplot (d) shows the $c2$ correction map; for comparison we showed in subplot (e) the image obtained by histogram stretching.

For numerically evaluation of our method we considered the histogram stretching method and internal ISO

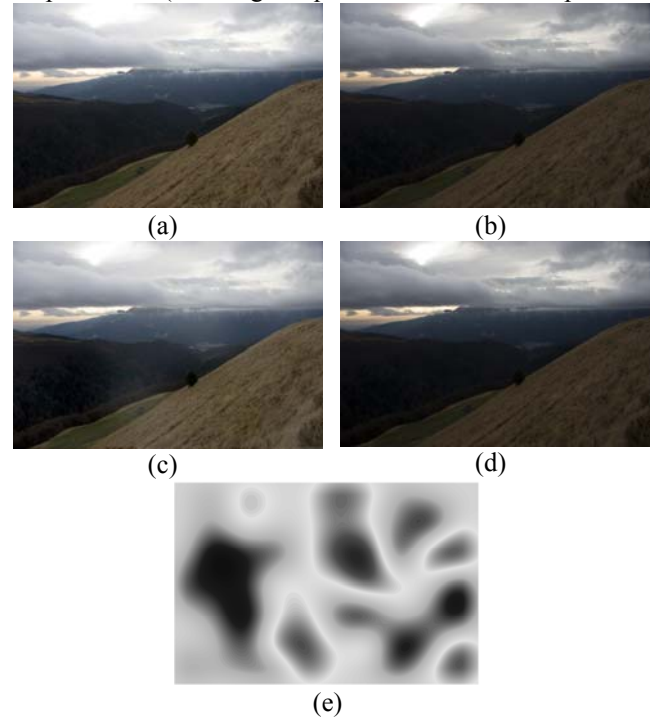amplification (i.e. image acquired with the small exposure

(a)   (b)

(c)   (d)

(e)

Figure 2: Low–light image amplification. The ideal image (acquired with tripod mounted camera) (a), original underexposed image (b), image resulted after applying our algorithm (c), image obtained by histogram stretching (d) and c_2 coefficient map (value–stretched to maximum for displaying -e). The histogram stretch does almost nothing to this image, while our method produces one extremely similar with the reference one.
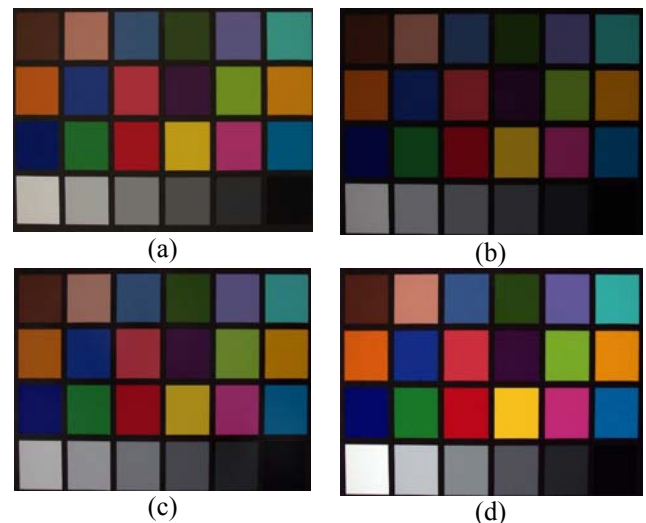

(a)   (b)

(c)   (d)

Figure 3. Low–light image amplification. The subplots have the same significance as in Fig. 2. On this artificial set, the image obtained by histogram stretching presents more pleasant colors, even that our algorithm produce an image closer to the reference one.

time, but with higher ISO). The methods were applied on a set of static images with scenes in which objects were manually segmented. The images were taken on a tripod and for each scene, the low-light image and the normally exposed image are available. Overall we used 3 different cameras (low consumer, medium consumer and high-end mobile phone). There are 104 images of 4000x3000 resolution underexposed with E_V=-2 and 112 with E_V=-1 and a total number of 616 patches (that were uniform enough) marked. The results are presented in tables 3 and 4. Supplementary, we counted in how many images there were regions with saturated (e.g. higher than 252), incorrect values.

The histogram stretching is the classical method (see [43], chapter 3.3), while for ISO we used the internal camera amplification (i.e. same exposure time as the underexposed image for our method, double S factor for E_V=-1 and quadruple for E_V=-2).

For comparison we considered typical reference measures, like $\bar{\varepsilon}$ (mean of absolute differences between the reference image and the processed images, given in intensity levels), ε_{max} (maximum difference between the mean of selected patches, also given in pixels) and the number of saturated areas, N_{sat}. For more thoroughly evaluation a no reference perceptual metric δS was added.

The last metric is based on the measure S (derived in [44]) so to be highly correlated with human mean opinion score:

$$ S = \frac{L}{\left(\sum_{R_b}\left|D_{R_b}\right|^{\beta}\right)^{\frac{1}{\beta}}} ; D_{R_b} = \left(\sum_{e_i \in R_b}\left|\frac{w(e_i)}{w_{JNB}(e_i)}\right|^{\beta}\right)^{\frac{1}{\beta}} \quad (20) $$

where β is *3.6* (extracted by psycho visually experiments) and L is the number of blocks, R_b, used of size 64x64. Each block is taken on the Sobel edge image e_i; $w(e_i)$ is the total edge width in the given block computed by counting the number of pixels with increasing grayscale values in one direction of the edge pixel while counting the number of pixels with decreasing grayscale values in the other direction. having width has small values in sharp images. $w_{JNB}(e_i)$ integrate in the measure the human perception as it has the meaning of the minimum edge width where a human objerver would notice blur (just noticeable blur). Since the actual measure depends on the image content, we considered as reference image, the acquired low light image, where the found measure is S_t and we computed δS as a percentage of increase (decrease) from the reference image:

$$ \delta S = 100\frac{2\left(S_t - S_{ref}\right)}{\left(S_t + S_{ref}\right)} \quad (21) $$

Obviously higher values for δS means better image.

Regarding the results showed in tables 3 and 4, one may notice that the proposed method outperformed the classical histogram stretching (always in terms of mean error, number of saturated areas and partially with respect to the perceptual metric), results easy explainable by the fact that the latter method simply targets a histogram type without using any information on the scene. The internal ISO amplification provided more accurate colors in general – smaller errors (easy explainable since it benefits from tuning with knowledge on the specific internal DSC processing), but it produces quite often saturated areas. Regarding the no-perceptual reference metric, δS, it gives an idea about the amount of noise existing in the final image (and amplification of noisy image produce it) and the local contrast provided; the images less underexposed have better

TABLE 3: OBJECTIVE MEASURES ON THE LOW LIGHT AMPLIFICATION ALGORITHM WHEN UNDEREXPOSING WAS E_V=-1. $\bar{\varepsilon}$ IS THE MEAN OF ABSOLUTE DIFFERENCES BETWEEN THE TRIPOD MOUNTED REFERENCE IMAGE AND THE PROCESSED IMAGES; ε_{max}, IS COMPUTED AS THE MAXIMUM DIFFERENCE BETWEEN THE MEAN OF THE PATCHES (OVER THE

ENTIRE TEST SET OUT OF A POSSIBLE MAXIMUM OF 255 INTENSITY LEVELS) AND IT EXCLUDES SATURATED AREAS; THE LAST ENCOUNTERS ARE GIVEN AS N_{sat}. VALUES δS ARE BASED ON NO-REFERENCE PERCEPTUAL METRIC FROM [44]. THERE WERE 112 IMAGES WITH 364 MANUALLY MARKED PATCHES.

Method	$\bar{\varepsilon}$ [lev]	ε_{max} [lev]	N_{sat}	δS [%]
Current	10.24	22	2	9.06
Histogram stretching	12.12	38	12	3.4
Internal ISO	7.15	17	15	7.63

TABLE 4: OBJECTIVE MEASURES ON THE LOW LIGHT AMPLIFICATION ALGORITHM WHEN UNDEREXPOSING WAS E_V=-2. THERE WERE 104 IMAGES WITH 352 MANUALLY MARKED PATCHES.

Method	$\bar{\varepsilon}$ [lev]	ε_{max} [lev]	N_{sat}	δS [%]
Current	15.12	35	4	-8.29
Histogram stretching	18.85	61	16	-5.67
Internal ISO	11.36	27	21	-11.71

contrast than noise, while for high underexposing, noise becomes dominant (for all solutions).

Specifically for the *Ev=-2* case, where the internal ISO amplification provide better perceptual score, the explanation lies in the designed tendency of the internal ISO amplification algorithm to provide maximum possible contrast by using the entire gamut. This trait, while it leads to the increase of the perceptual metric *S*, comes with the disadvantage of exceeding the given range and forming burned images. As N_{sat} shows, the incidence of such areas is much higher in the case of ISO amplification. On the other hand, the use of LIP models impedes the intensity overflow but produces less contrast in other areas. To avoid contrast diminishing the solution at hand is to reduce size of the blur kernel radius used for smoothing *c2* map.

The use of the LTIP models with their closing property ensures that we will never exceed the given range. Furthermore, with the cost of some extra operations, the refined search of the c_2 factor makes the method to provide a better dynamic range and local contrast than usual.

The duration of the proposed method is in average 0.232 *10^{-7} sec/pixel in single core Matlab implementation on an Intel i7 at 2.7 GHz.

VI. CONCLUSIONS

In this paper we have summarized our contribution to the advance of parametric logarithmic-type image processing models. From a mathematical point of view, these models form definite structures, namely vector or cone space. The most important LIP property is that of closing. This property ensures special behaviors near the edges of the definition set. Applied on logarithmic-like models, this property shows similarity with Stevens effect of the human visual system and thus with gamma-like function of digital still camera.

From the application point of view, non-linearity localized especially near the boundary of the value domain makes them suitable for processing images that have important part of the histogram in these ranges; these are images acquired in extreme lighting. We have shown the usability of the proposed framework by describing an application for digital still cameras- low-light enhancement - that showed results superior to the state of the art methods.

Regarding the further continuation paths, the algorithms are currently in a process of optimization, including adaptation for ASIC (Application Specific Integrated Circuit) acceleration. The latter process is rather easy since the framework is pixel-wise oriented, hence powerfully parallelization may be used. Also another DSC core algorithm that is non-linear is the white balance. We will investigate if this part can benefit from the LTIP model properties.

REFERENCES

[1] J. S. Lim, "Two Dimensional Signal and Image Processing", Upper Saddle River, Prentice Hall, New Jersey, US, 1990.

[2] M. Jourlin, J. C. Pinoli, "A model for logarithmic image processing", Journal of Microscopy, vol. 149, no. 1, pp. 21– 35, 1988.

[3] V. Pătraşcu, I. Voicu, "An algebraical model for gray level images", in: Proceedings of the Exhibition on Optimization of Electrical and Electronic Equipment, OPTIM, Braşov, Romania, pp. 809 – 812, 2000.

[4] C. Vertan, A. Oprea, C. Florea, L. Florea, "A pseudo-logarithmic framework for edge detection", in: J. B.-T.et al (Ed.), Advanced Concepts for Intelligent Vision Systems, Vol. 5259 of LNCS, Springer Verlag, pp. 637 – 644, 2008.

[5] K. Panetta, E. Wharton, S. Agaian, "Human visual system-based image enhancement and logarithmic contrast measure", IEEE Transactions on Systems, Man, and Cybernetics - part B: Cybernetics, vol. 38, no. 1, pp. 174-188, 2008.

[6] G. Deng, "A generalized logarithmic image processing model based on the Giga-vision sensor model", IEEE Transactions on Image Processing , vol. 21, no. 3, pp. 1406-1414, 2012.

[7] C. Florea, C. Vertan, L. Florea, A. Sultana, "Non-linear parametric derivation of contour detectors for cellular images", in: Proceedings of IEEE International Symposium on Signals, Circuits and Systems, ISSCS, Vol. 2, IEEE, Iasi, Romania, 2009, pp. 1 – 4.

[8] C. Florea, L. Florea, "A parametric non-linear algorithm for contrast based auto-focus", IEEE 7th International Conference on Intelligent Computer Communication and Processing, pp. 267 – 271, 2011.

[9] A. V. Oppenheim, "Superposition in a class of non-linear system", Tech. rep., Research Laboratory of Electronics, M.I.T., Cambridge, U.S. 1965.

[10] A. V. Oppenheim, "Generalized superposition", Information and Control, vol.11, no. 5,6, pp. 528 – 536, 1967.

[11] J. Hefferon, "Linear Algebra", web edition, 2008, http://joshua.smcvt.edu/math/hefferon.html.

[12] M. Jourlin, J. C. Pinoli, "Logarithmic image processing", Acta Stereologica, vol. 6, pp. 651 – 656, 1987.

[13] Q. Z. Wu, B. S. Jeng, "Background subtraction based on logarithmic intensities", Pattern Recognition Letters, vol. 23, no. 13, pp. 1529 – 1536, 2002.

[14] M. Jourlin, J. C. Pinoli, "Image dynamic range enhancement and stabilization in the context of the logarithmic image processing model", Signal Processing, vol. 41, no. 2, pp. 225 – 237, 1995.

[15] G. Deng, L. W. Cahill, G. R. Tobin, "A study of logarithmic image processing model and its application to image enhancement", IEEE Transactions on Image Processing, vol. 4, no. 4, pp. 506 – 512, 1995.

[16] V. Patrascu, V. Buzuloiu, Color image enhancement in the framework of logarithmic models, in: Proceedings of the 8th IEEE International Conference on Telecommunications, Vol. 1, Bucharest, Romania, pp. 199– 204, 2001.

[17] J. C. Pinoli, J. Debayle, Logarithmic adaptive neighborhood image processing (lanip): Introduction, connections to human brightness perception, and application issues, EURASIP Journal on Advances in Signal Processing, vol. 1, 2007 article ID 36105, doi:10.1155/2007/36105,.

[18] G. Deng, "An entropy interpretation of the logarithmic image processing model with application to contrast enhancement", IEEE Transactions on Image Processing, vol. 18, no. 5, 1135 – 1140, 2009.

[19] C. Florea, C. Vertan, "Piecewise linear approximation of logaritmic image processing models for dynamic range enhancement", Scientific Bulletin of University Politehnica of Bucharest, vol. 71, no. 2 pp. 3 – 15, 2009.

[20] K. Panetta, Y. Zhou, S. Agaian, E. Wharton, "Parameterized logarithmic framework for image enhancement", IEEE Transactions on Systems, Man, and Cybernetics - part B: Cybernetics, vol. 41 no. 2, pp. 460 – 472, 2011.

[21] R. Ramanath, W. Snyder, Y. Yoo, M. Drew, "Color image processing pipeline: A general survey of digital still camera processing", IEEE Signal Processing Magazine, vol. 22 no. 1, pp. 34 – 43, 2005.

[22] A. PH2.5-1960, "American standard method for determining speed of photographic negative materials (monochrome, continuous tone)", United States of America Standards Institute, 1960.

[23] R. Jacobson, S. Ray, G. G. Attridge, N. Axford, "Manual of Photography: Photographic and Digital Imaging", Focal Press, Oxford ; Boston, MA, 2000.

[24] J. Nakamura (Ed.), "Image sensors and signal processing for digital still cameras", Academic Division of T&F Informa, Taylor and Francis Group, Boca Raton, Florida, USA, 2006.

[25] Y. C. Chang, J. F. Reid, "RGB calibration for color image analysis in machine vision", IEEE Transactions on Image Processing, vol. 5 no. 10, pp. 1414–1422, 1996.

[26] P. Debevec, J. Malik, "Recovering high dynamic range radiance maps from photographs", in: ACM SIGGRAPH Proceedings of the 24th Annual Conference on Computer Graphics and Interactive Techniques, Los Angeles, US, pp. 369–378, 1997.

[27] M. D. Grossberg, S. K. Nayar, "High dynamic range from multiple images: Which exposures to combine?", in: Proceedings of IEEE Workshop on Color and Photometric Methods in Computer Vision at ICCV, Nice, France, 2003.

[28] S. Mann, R. Picard, "Being 'undigital' with digital cameras: Extending dynamic range by combining differently exposed pictures", in: Proceedings of IS&Ts 48th, Vol. 1, Washington D.C, US, pp. 422–428, 1995.

[29] T. Mitsunaga, S. K. Nayar, "Radiometric self calibration", in: Proceedings of IEEE Conference on Computer Vision and Pattern Recognition, CVPR, Vol. 1, Ft. Collins, S.U.A, pp. 374–380, 1999.

[30] F. Xiao, J. Pincenti, G. John, K. Johnson, "Camera motion and mobile imaging", in: Proceedings of the SPIE-IST Electronic-Imaging, Vol. 6502, 2007.

[31] K. Sato, S. Ishizuka, A. Nikami, M. Sato, "Control techniques for optical image stabilizing system", IEEE Transactions on Consumer Electronics, vol. 39, no. 3, pp. 461 – 466, 1993.

[32] F. Xiao, J. Pincenti, J. Farrell, "Camera motion and effective spatial resolution", in: Proceedings of International Congress of Imaging Science, Vol. 1, May, pp. 33–36, 2007.

[33] S. Perstel, E. Pozniansky, O. Meitav, "Camera optimization techniques that take camera and scene motion into account", US Patent, 7546026, 2007.

[34] C. Florea, F. Albu, C. Vertan, A. Drımbarean, "Logarithmic tools for in-camera image processing", in: Proceedings of 16th IET Irish Signals and Systems Conference, Galway, Ireland, pp. 394–399, 2008.

[35] F. Albu, E. Steinberg, A. Drımbarean, C. Florea, A. Zamfir, P. Corcoran, V. Poenaru, "Image processing method and apparatus", US Patent, 20080219581, 2008.

[36] M. Aguilar, W. Stiles, "Saturation of the rod mechanism of the retina at high levels of stimulation", Optica Acta, vol. 1 no. 11, pp. 59–65, 1954.

[37] M. D. Grossberg, S. K. Nayar, "Modeling the space of camera response functions", IEEE Transactions on Pattern Analysis and Machine Inteligence, vol. 26, no.10, pp. 1272 –1282, 2004.

[38] C. A. Poynton, "Rehabilitation of gamma", Proc. SPIE vol. 3299 no. 232, doi:10.1117/12.320126.

[39] J. Stevens, S. Stevens, "Brightness functions: Effects of adaptation", Journal of the Optical Society of America, vol. 53, pp. 375–385, 1963.

[40] F. Dunn, M. Lankheet, and F. Rieke, "Light adaptation in cone vision involves switching between receptor and post-receptor sites", Nature, vol. 449, no. 7162, pp. 603-606, 2007

[41] D. Hubel, "Eye, Brain, and Vision", Scientific American Library, 1995

[42] S. J. Russell, P. Norvig, "Artificial intelligence: a modern approach", Upper Saddle River, New Jersey: Prentice Hall, 2003.

[43] R. C. Gonzales, R. E. Woods, "Digital Image Processing", Addison Wesley, Reading, Massachusetts, US, 1992.

[44] R. Ferzli, L. J. Karam, "A no-reference objective image sharpness metric based on the notion of just noticeable blur (JNB)", IEEE Transactions of Image Processing, vol. 19 no. 4, pp. 717 – 728, 2009.